

Plasmons in Topological Insulators

O. Roslyak, Godfrey Gumbs
*Department of Physics and Astronomy,
 Hunter College, City University of New York,
 695 Park Avenue, New York, NY 10065, USA**

Danhong Huang
*Air Force Research Laboratory, Space Vehicles Directorate,
 Kirtland Air Force Base, NM 87117, USA
 (Dated: December 2, 2024)*

We calculated the edge-plasmon excitation spectrum within the anti-crossing bulk bandgap region for an inverted **HgTe/CdTe** quantum well by employing the Bernevig, Hugues and Zhang (BHZ) model within the random-phase approximation (RPA). Our proposed model system consists of a single component electron helical liquid (HL) in a semi-infinite quantum well, in which a topological state that is localized around the system edge can exist. With linearly-polarized incident light as a perturbation to such a single component HL, the unique charge dynamics for collective excitation of these edge-bound electrons with broken time-reversal symmetry is investigated. The plasmon dispersion $\omega_p(q)$ of the single component HL has the form $\omega_p(q) \sim -\omega_0 q \ln(qa)$ in the long-wavelength limit, which is in sharp contrast with $\omega_p(q) \sim -\omega_0 \sqrt{-\ln(qW)}$ for a one-dimensional electron gas (1DEG) in a quantum-wire system. Here, the plasmon wave number in a conventional 1DEG is scaled with a characteristic width W , while that in our model system is scaled with a lattice constant a . Similar to interband plasmons in a metallic armchair graphene nanoribbon, ω_0 is found to be independent of the linear electron density for the intraband plasmon in our system. Besides the spin factor of two and W scaling for the wave number, the dispersion relation for the collective excitation of the two component HL is the same as that in an armchair graphene nanoribbon. The particle-hole excitation region in our system is found to be collapsed into a straight line, instead of a wide region for a conventional 1DEG. The plasmon energies of the two and single-component HL are spectrally separated although the same particle-hole excitation region is shared by both of them.

I. INTRODUCTION

Topological insulators (TIs) are found to be a new class of materials which possess insulating (large bandgap) states in the bulk but conducting edge states on their surfaces. Only states along edges of TIs have non-flattened dispersion (extended states) within a bulk bandgap, thereby allowing for charge and spin currents under zero bias [1]. The bulk bandgap of a TI is usually large enough to be comparable to room temperature, which makes TIs thermally stable and a good candidate for high-power electrical and optical applications. One example of such TIs is the so-called three-dimensional (3D) TI, e.g., **Bi₂Te₃** crystals. These 3DTIs are 3D band insulators possessing two-dimensional (2D) conducting surface states. Additionally, there exist 2DTIs, in which the conducting states are localized close to all edges of a slab in real space and display a well-defined Dirac cone in momentum space. In this paper, we confine our attention to another predicted type of TI which has already been demonstrated in an inverted **HgTe/CdTe** (also called type-III) quantum well when the well thickness exceeds 6.3 nm. The type-III quantum well is formed by sandwiching a thin narrow-bandgap **HgTe** layer between two thick wide-bandgap **CdTe** layers in the growth (z) direction. Bulk **HgTe/CdTe** is a semimetal with zero bandgap. The quantum-size effect from a quantum well introduces a finite but very small bandgap to a **HgTe/CdTe** layer. As expected, the induced bandgap in a **HgTe/CdTe** layer decreases with the layer thickness. For an inverted **HgTe/CdTe** quantum well, the usual lower p -type Γ_8 -band moves above the s -type Γ_6 -band around the center of the Brillouin zone to create an anti-crossing bulk bandgap as well as a negative effective mass for conduction electrons at the same time. This **HgTe/CdTe**-based TI is one type of 2DTI. A semi-infinite quantum well extends infinitely in the x direction but is still confined within a half-plane ($y < 0$) in the y direction. Consequently, there always exists one conducting channel (helical edge state) for spin-up or spin-down electrons along the edge ($y = 0$) of a half- xy plane (with a finite thickness in the z direction). This means that we may easily assign a spin component to a current if we know its flowing direction. The switching from a left to a right circular-polarization

*Electronic address: avroslyak@gmail.com

of incident light is expected to change the flow direction of a photocurrent [2]. This helical state spans over a quantum well in the z direction and forms a quasi-one-dimensional electron gas (quasi-1DEG). The energy dispersion of the helical state lies within the anti-crossing bandgap region of an inverted **HgTe/CdTe** quantum well. The theoretical description of this type of topological states is given by the model of Bernevig, Hugues and Zhang (BHZ) [3, 4].

The spin dynamics of TIs have received a great deal of attention, including a topological quantum phase transition in a tunable spin-orbit system [5], spin-polarized electrical current [6] and a photocurrent induced by circularly-polarized incident light [2]. However, unique properties of charge dynamics in the same systems are much less known. The goal of this paper is to investigate the charge dynamics of collective excitations of those edge-bound electrons in the presence of a linearly-polarized incident light. In a simplified model, 3DTIs were studied [6, 7] by assuming that the surface bound states form a 2D electron gas (2DEG). In addition, the dispersions of those surface states are simply taken to be Dirac cones similar to those in graphene, and the conduction and valence bands are made of states with different helicities (spins). As it is known for graphene, the undamped plasmons can exist only by including both interband and intraband transitions [8]. Therefore, we expect that the collective excitation of electrons with a given helicity (broken time-reversal symmetry) will be severely Landau damped. The symmetry breaking is often accompanied by some unexpected physical effects. In the presence of a perpendicular magnetic field (broken time-reversal symmetry), the splitting of edge magnetoplasmon modes for a 2DEG on a half-plane was previously predicted [9].

To study the charge dynamics of undamped collective excitations of electrons having a given helicity, we employ a 2DTI model system [3, 4] instead of 3DTIs [6, 7]. For the 2DTI system, the BHZ model predicts the existence of both insulating bulk and conducting $(1, 0)$ -edge states in an inverted **HgTe/CdTe** quantum well, similar (but not identical) to those in a metallic armchair graphene nanoribbon (ANR). In a graphene ANR, the plasmon excitations are excited by interband transitions only [10]. Unlike those in a 2DTI system, electronic states in a graphene ANR are not localized around the two ribbon edges. Moreover, both helical branches contribute to plasmon excitations. This makes the plasmon dispersion in a graphene ANR almost identical to that of a conventional 1DEG.

In this paper we investigated the effect of wave function localization in a semi-infinite 2DTI system on the collective excitation of electrons. Our calculated plasmon dispersion is compared with those in a conventional 1DEG [11] and in a metallic graphene ANR. Following the work by Zhang *et al.* [12], we adopt the terminology that an n -component helical liquid (HL) contains n -time reversal pairs of fermions. These n -component HL states are localized on different edges of a quantum well. For a semi-infinite quantum well, on the other hand, we only need to consider a single fermion of the pair to calculate the Coulomb excitation of electrons. The contributions from a single (for a given electron helicity) and two component HL to the plasmon excitation are explored. Our calculations indicate that ANR and the semi-infinite 2DTI system can be considered to be two and single component HL, respectively, in calculating the charge dynamics of collective excitations.

The rest of the paper is organized as follows. In Sec. II, we calculated the edge-localized helical states of electrons and their energy dispersion in a semi-infinite inverted **HgTe/CdTe** quantum well. In Sec. III, the dispersion of edge-plasmon excitations in our system with broken time-reversal symmetry is calculated and compared with that in a conventional one-dimensional electron gas and in a metallic armchair graphene nanoribbon. Finally, the conclusions of the paper are given briefly in Sec. IV.

II. FORMALISM OF 2DTI IN **HgTe/CdTe** QUANTUM WELL

To study the collective electronic excitations, let us start with the BHZ model for the electron band structure near the center $\Gamma_k = (0, 0)$ of the first Brillouin zone. We assume that the quantum well is infinite along the x direction and finite or semi-infinite along the y direction. The width of the well is given implicitly within the parameters $[A, B$ and Δ in Eq. (1)] of the model Hamiltonian. The “ansatz” wave function is taken to be $\exp(ikx)$ in the x direction. Along the y direction, we discretize the spatial position as $y = ja > 0$ with $j = 1, 2, \dots, N$ being a positive integer and a being the lattice constant, where N is the total number of sites assumed for numerical simulations in the y direction, and is taken sufficiently large to ensure that two edge topological states do not overlap each other. The wave number k in the x direction is given in units of $k_B = \pi/a$, leading to discrete spatial positions along the x axis as $x = \ell a$ with $\ell = -N/2, \dots, -2, -1, 0, 1, 2, \dots, N/2$ being an integer.

According to Ref. 3, the Hamiltonian describing electronic states in a **HgTe/CdTe** (type-III) quantum well can be written as a block-tridiagonal matrix

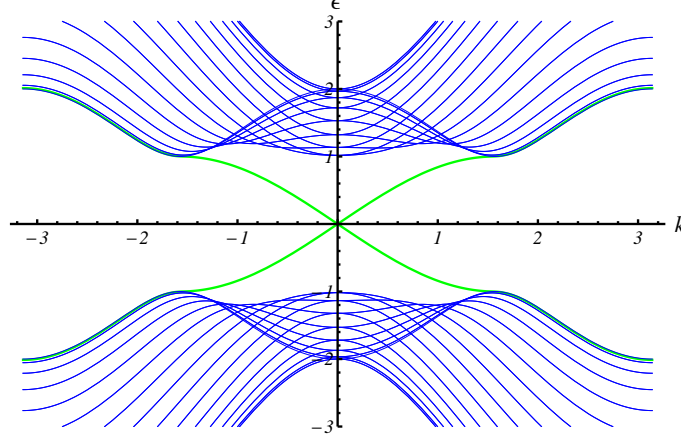


FIG. 1: (Color online) Full band structure $\varepsilon(k)$ of a 2DTI with $\Delta = 2B$, $A = B = 1$ and $N = 30$. The blue curves correspond to the bulk modes while the two green curves represent the topological surface states. Each state is doubly degenerate with respect to the two eigenvalues of the σ_x matrix.

$$\mathcal{H} = \begin{pmatrix} \ddots & \ddots & \ddots & 0 & 0 & 0 & 0 \\ 0 & t & \varepsilon & (t^T)^\dagger & 0 & 0 & 0 \\ 0 & 0 & t & \varepsilon & (t^T)^\dagger & 0 & 0 \\ 0 & 0 & 0 & t & \varepsilon & (t^T)^\dagger & 0 \\ 0 & 0 & 0 & 0 & \ddots & \ddots & \ddots \end{pmatrix}_{4N \times 4N}, \quad (1)$$

$$\varepsilon = A \sin(k) \Gamma_1 + [\Delta - 4B + 2B \cos(k)] \Gamma_5,$$

$$t = -\frac{iA}{2} \Gamma_2 + B \Gamma_5.$$

Here, the elements of the Clifford algebra are expressed in terms of $\Gamma_1 = \sigma_x \otimes \sigma_z$, $\Gamma_2 = -\sigma_y \otimes \sigma_0$ and $\Gamma_5 = \sigma_z \otimes \sigma_0$ with σ_i denoting the Pauli matrices. Additionally, A , B , Δ in Eq. (1), which are scaled by $\hbar k_B v_F$ with $v_F \sim c/1000$ being the Fermi velocity expressed in terms of the speed of light c , are the material parameters dependent on the quantum well width. The form of the Hamiltonian in Eq. (1) implies that the associated wave function vanishes at edges.

The calculated energy dispersion corresponding to Eq. (1) is presented in Fig. 1. For $0 < \Delta/B < 4$, two localized states at the boundaries are obtained, which may be expressed in terms of a linear combination of the ansatz wave functions [13]

$$\begin{aligned} \Psi_{j,l} &= \frac{1}{\sqrt{Na}} \sum_k \psi_j^>(k) e^{ikl} + \frac{1}{\sqrt{Na}} \sum_k \psi_j^<(k) e^{-ikl} \\ &= \frac{1}{\sqrt{Na}} \sum_k [\rho(k)]^j e^{ikl} \frac{1}{\sqrt{Na}} \sum_k [\rho(k)]^{N+1-j} e^{-ikl}, \end{aligned} \quad (2)$$

where the helical states are chosen to be the eigenstates defined by $\Gamma_1 |\pm\rangle = \pm |\pm\rangle$. The analytic solutions of Eq. (2) may be obtained by substituting the above ansatz wave functions into Eq. (1) and considering the identity $[i\Gamma_5 \Gamma_2, \Gamma_1] = 0$. This yields

$$\begin{aligned} \psi_j^>(k) &= (c_{+,1}^> [\rho_1(k)]^j + c_{+,2}^> [\rho_2(k)]^j) |+\rangle \\ &\quad + (c_{-,1}^> [\rho_1(k)]^{-j} + c_{-,2}^> [\rho_2(k)]^{-j}) |-\rangle, \\ \psi_j^<(k) &= (c_{+,1}^< [\rho_1(-k)]^{N+1-j} + c_{+,2}^< [\rho_2(-k)]^{N+1-j}) |-\rangle \\ &\quad + (c_{-,1}^< [\rho_1(-k)]^{-N-1+j} + c_{-,2}^< [\rho_2(-k)]^{-N-1+j}) |+\rangle. \end{aligned} \quad (3)$$

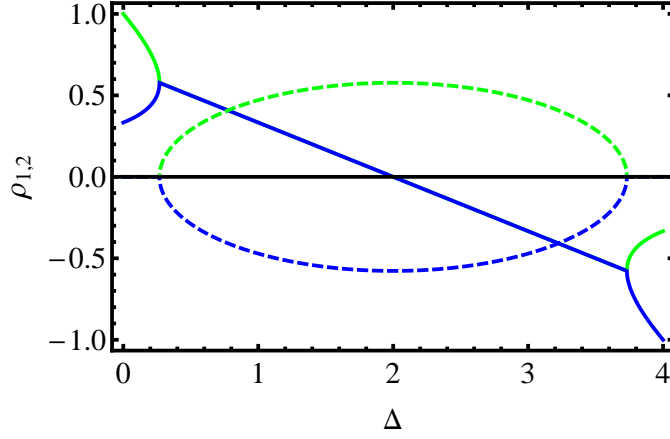


FIG. 2: (Color online) Based on Eq. (5) the real (solid curves) and imaginary (dashed curves) parts of ρ_1 (green) and ρ_2 (blue) at $k = 0$ as a function of Δ/B for $A = B = 1$.

The wave function corresponding to $|+\rangle$ in Eq. (3) is related to the energy dispersion $E_+(k) = A \sin(k)$, while that corresponding to $|-\rangle$ is associated with $E_-(k) = -A \sin(k)$, as shown by two green curves in Fig.1. The deviation from the sine function becomes significant once $E_{\pm}(k)$ merges with the bulk modes (shown as blue curves). Parameters $\rho_1(k)$ and $\rho_2(k)$ in Eq. (3) are defined by

$$\rho_{1,2}(k) = \frac{-\Omega(k) \pm \sqrt{\Omega^2(k) + A^2 - 4B^2}}{A + 2B}, \quad (4)$$

$$\Omega(k) = \Delta - 2B[2 - \cos(k)]. \quad (5)$$

For $A = B = 1$ and $k = 0$, the variation of these parameters with respect to Δ/B is displayed in Fig. 2.

Since our interest is limited to calculating the plasmon dispersion in the long-wavelength limit, we would only consider the case with $k \ll 1$. This leads to the approximate expression $E_{\pm}(k) \approx \pm Ak$, and $\rho_{1,2}(k) \approx \rho_{1,2}(0)$ become k -independent at the same time. For $\Delta = 2B$, we find $\rho_{1,2} = \pm i/\sqrt{3}$.

The coefficients $c_{\pm,\alpha}$ with $\alpha = 1, 2$ in Eq. (3) may be determined from the boundary conditions as well as the wave function normalization condition. By choosing $N \gg 1$, the condition for a finite-valued wave functions requires $c_{-,\alpha}^> = c_{+,\alpha}^< = 0$. Moreover, the vanishing boundary conditions lead to $c_{+,1}^> + c_{+,2}^> = 0$ and $c_{-,1}^< + c_{-,2}^< = 0$. After normalizing the wave functions in Eq. (3), we find $c_{+,1}^> = c_{-,1}^< = 2/\sqrt{3}$. Therefore, the wave functions do not overlap and are localized on opposite boundaries. In addition, the eigenvalues of the spin state of σ_x are related to the sign of the group velocity, i.e., $\psi_j^>$ corresponds to $E_+(k)$ while $\psi_j^<$ is related to $E_-(k)$. This pair of fermions constitutes a 1-component HL, and is connected by the time-reversal symmetry. For a semi-infinite quantum well with $N \rightarrow \infty$ and $\rho_{1,2} = \pm i/\sqrt{3}$, on the other hand, we are left with a single helical state localized at the $j = 0$ boundary

$$\psi_j^> \approx \frac{2(i)^j}{(\sqrt{3})^{j+1}} [1 - (-1)^j] |+\rangle, \quad (6)$$

$$E_+(k) \approx Ak.$$

If the material parameters $|\rho_{1,2}| > 1$ are chosen, one would retain the left mover $\psi_j^<$ proportional to $|-\rangle$ as the proper solution. For a 2-component HL, we must consider two helical states on each edge.

III. PLASMONS IN HL COMPARED WITH 1DEG

Based on the calculated full band structure from the BHZ model, we will further study the electron screening dynamics from the dielectric function of a 2DTI system. Specifically, we will consider a semi-infinite type-III quantum well, in which only one helical state can occur and is localized around the edge ($y = 0$) of the system. As a result, there exist only intraband transition in our system. For the wave function given by Eq.(6), the plasmon excitation

dispersion $\omega_p(q)$ within the random-phase approximation (RPA) is determined by the zero of the following dielectric function

$$\begin{aligned}\epsilon(q, \omega) &= 1 - V_{+,+,+,+}(q) \Pi_{+,+}(q, \omega + i0^+) \\ &= 1 - \frac{1}{\pi} \frac{q V_{+,+,+,+}(q)}{\hbar\omega - Aq} + iq V_{+,+,+,+}(q) \delta(\hbar\omega - Aq),\end{aligned}\quad (7)$$

where the noninteracting polarization function at zero temperature is given by

$$\begin{aligned}\Pi_{+,+}(q, \omega + i0^+) &= \frac{1}{N} \sum_k \frac{\theta(k+q) - \theta(k)}{E_+(k) - E_+(k+q) + \hbar\omega + i0^+} \\ &= \frac{2}{2\pi} \frac{q}{\hbar\omega - Aq + i0^+}.\end{aligned}\quad (8)$$

Here, $\theta(x)$ is the unit step function and $E_F = 0$ is assumed for the Fermi energy. The prefactor of two in Eq. (8) accounts for the double degeneracy of the bands. Very importantly, the time-reversal symmetry is broken in Eq. (8) for the response function, i.e., $\Pi_{+,+}(q, \omega + i0^+) \neq \Pi_{+,+}^*(q, -\omega + i0^+)$. The Coulomb matrix element introduced in Eq. (7) is given by [14]

$$V_{+,+,+,+}(q) = \frac{2e^2}{\epsilon_s a} \sum_{j=1}^{\infty} \sum_{j'=j+1}^{\infty} |\psi_j^>|^2 |\psi_{j'}^>|^2 K_0[q(j' - j)], \quad (9)$$

where $K_0(x)$ is the modified Bessel function of the second kind, $\epsilon_s = \epsilon_0 \epsilon_b$ and ϵ_b is the dielectric constant of the host material. If it is not explicitly stated, our parameters of choice are $A = B = 1$ and $\Delta = 2B$ in this paper. For this parameter choice, the summation in Eq. (9) can be carried out explicitly to give

$$\begin{aligned}V_{+,+,+,+}(q) &= \frac{2e^2}{\epsilon_s a} \int_0^{\infty} \frac{12 \cos(qt) dt}{5\sqrt{1+t^2} [41 - 9\cos(2qt)]} \\ &\approx \frac{e^2}{\epsilon_s a} \frac{3}{20} K_0(q).\end{aligned}\quad (10)$$

Here, the validity of the last approximation is demonstrated in Fig.3, and the prefactor can be calculated, by using the fine-structure constant and $\epsilon_b = 7$ for HgTe, as $e^2 k_B / \epsilon_s A = 4\pi \times 0.001 (\hbar k_B v_F / A) (c/v_F) \approx 4\pi$.

The imaginary part of the dielectric function in Rq. (7) yields the boundary $\hbar\omega_{p-h} = Aq$ for the particle-hole excitation region, while zeroes of the real part give rise to the plasmon dispersion relation

$$\hbar\omega_p(q) = Aq \left[1 + \frac{1}{\pi A} V_{+,+,+,+}(q) \right]. \quad (11)$$

In the long-wavelength limit with $qa \ll 1$, we obtain $\text{Re}[\Pi_{+,+}(q, \omega + i0^+)] = q/\pi\hbar\omega + \mathcal{O}(q^2)$ as a leading-order result. In conjunction with Eq. (10), this leads to the explicit plasmon dispersion relation

$$\begin{aligned}\omega_p(q) &= -\omega_0 q \ln(q) + \mathcal{O}(q^2), \\ \hbar\omega_0 &= \frac{e^2}{\pi\epsilon_s a} \frac{3}{20}.\end{aligned}\quad (12)$$

Results from our calculations based on Eqs. (10), (11) and (12) are presented in Fig.4. It is found that $A = B = 1$ and $\Delta = 2B$ gives us the lower boundary of the plasmon excitation energy. This implies that the variations of A , B and Δ within the regime in which the topological edge state exists results in an increase in the plasmon energy.

Most inelastic scattering experiments measure the dynamic structure factor $\sim \text{Im}[\epsilon^{-1}(q, \omega)]$ or the inverse dielectric function. We display $\text{Im}[\epsilon^{-1}(q, \omega)]$ in Fig. 5 as a function of ω for chosen values of q . Clearly, the spectrum of

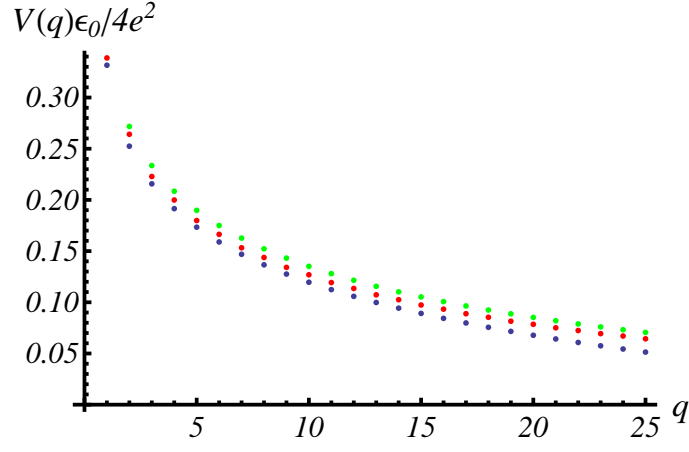


FIG. 3: (Color online) The q dependence (in units of the reciprocal inter-atomic spacing a) of the scaled Coulomb matrix element $V_{+,+,+,+}(q)/(4e^2/\epsilon_s a)$ in Eq. (9) evaluated between its upper $(3/40)K_0(q)$ (green) and lower bound $-(3/40)\ln(q)$ (black) for various values of the ratio Δ/B , where $A = B = 1$. The result for the approximate expression in Eq. (10) is given by red dots in the figure.

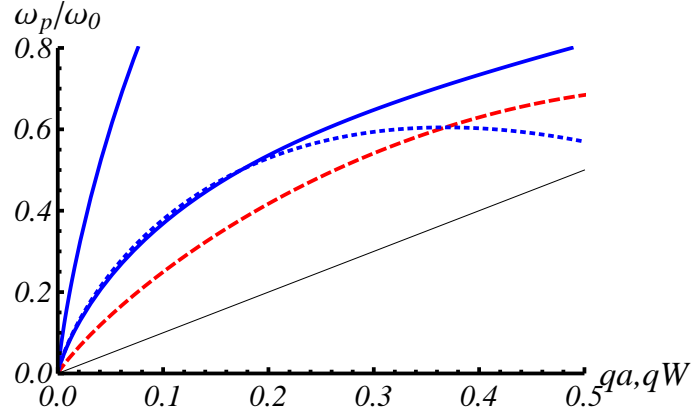


FIG. 4: (Color online) Scaled plasmon excitation energy $\omega_p(q)/\omega_0$ of 2DTI (blue solid curve) given by Eq. (11) with $A = B = 1$. The lower blue solid curve corresponds to $\Delta = 2B$, while the upper blue solid curve is for $\Delta = B$ or $\Delta = 3B$. The result of Eq. (12) is given by the dashed blue curve in the long-wavelength limit. The conventional 1DEG plasmon dispersion is indicated by a red dashed curve. The boundary for the particle-hole excitation region is represented by a thin black straight line.

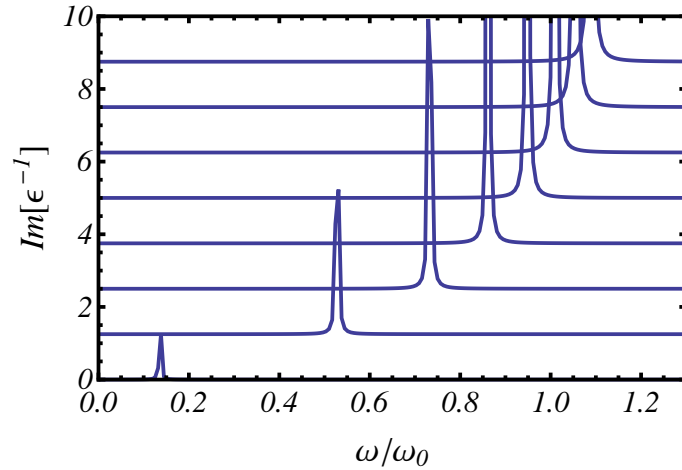


FIG. 5: Spectral function $\text{Im}[\epsilon^{-1}(q, \omega)]$ of single component HL in 2DTI as a function of ω/ω_0 with and chosen q . Here, the curves with different values for q are offset vertically for clarity.

$\text{Im}[\epsilon^{-1}(q, \omega)]$ is dominated by the plasmon resonance. The particle-hole excitation is not pronounced in this figure. Around the plasmon resonances, we can employ the plasmon-pole approximation $\text{Im}[\epsilon^{-1}(q, \omega)] \sim \beta_q \delta(\omega - \omega_p)$, where the plasmon weight is defined by

$$\beta_q = \frac{\pi}{[\partial \text{Re} \epsilon(q, \omega) / \partial \omega]_{\omega=\omega_p}} \quad (13)$$

$$= -\frac{\pi^2 \hbar \omega_0^2 q \ln^2(q)}{V_{+,+,+,+}(q)}. \quad (14)$$

Although varying the parameters of a 2DTI system from those producing the minimal $\omega_p(q)$ can increase the plasmon energy, it reduces the plasmon weight.

Now, let us compare our result with several known cases of 1DEG. For a conventional semiconductor quantum wire with a parabolic energy dispersion $E_0(k) = \hbar^2 k^2 / 2m^*$ for conduction electrons, the intraband plasmon dispersion in the long-wavelength limit can be written as [11, 14, 15]

$$\begin{aligned} \omega_p(q) &= \omega_0 q \sqrt{-\ln(q)} + \mathcal{O}(q^2), \\ \omega_0 &= \left(\frac{2v_F e^2}{\pi \hbar \epsilon_s W^2} \right)^{1/2} = \left(\frac{2n_{1D} e^2}{\epsilon_s m^* W^2} \right)^{1/2}, \end{aligned} \quad (15)$$

where n_{1D} and m^* denote the electron linear density and effective mass, respectively. For 1DEG, the wave vector q is scaled with the characteristic size W of the nanowire, i.e., $q \rightarrow qW$. The linear scaling of the plasmon frequency with the square-root of electron density as well as the high sensitivity to the wire characteristic size $\sim \sqrt{-\ln(qW)}$ are the unique properties of 1DEG in conventional semi-conducting nanowires. These properties are in sharp contrast with our result in Eq. (15) for localized quasi-1DEG in a 2DTI system.

For the conventional 1DEG, the plasmon weight is given by

$$\begin{aligned} \beta_q &\sim \frac{q [-\ln(q)]^{3/2}}{V_c(q)}, \\ V_c(q) &= \frac{2e^2}{\epsilon_s W} [K_0(q) + 1.972], \end{aligned} \quad (16)$$

which has different power dependence for the term $\sim \ln(q)$. Comparison of the plasmon weights are shown in Fig. 6 for both the TI-based and conventional 1DEG. From Fig. 6, we find that the plasmon weight in 2DTI is an order of magnitude larger than that of the conventional 1DEG. Consequently, a much more pronounced dynamical structure factor is expected for 2DTI [compare Fig. 5 here with Fig. 7 of Ref. [11]]. We also note that the particle-hole excitation spectrum exists in a wide region $k_F q / m^* - \hbar^{-1} E_0(q) < \omega_{p-h} < k_F q / m^* + \hbar^{-1} E_0(q)$ for a conventional 1DEG rather than a narrow line in 2DTI.

One of the striking features of 1DEG is that the RPA becomes exact for small value vectors q . This implies that the quasi-particles obtained from the exactly solvable linearized Tomonaga-Luttinger model agree with the calculated plasmon dispersion relation in the RPA [16]. In the case of a single-component HL for a 2DTI system, only one electron branch in the Tomonaga-Luttinger model should be included. The same argument can be applied to the plasmon dispersion in 2DTI as in conventional 1DEG but with no restriction for small q .

It is also very interesting to compare the results in our paper with similar ones for graphene-based nanostructures, where 1DEG is provided by chiral-state electrons. A detailed calculation using RPA for plasmon excitations in both armchair and zigzag edged graphene-based nanoribbons was carried out by Brey and Fertig [10], and only the armchair type was found to exhibit undamped plasmon excitations. The most interesting finding in Brey and Fertig's work is the presence of metallic nanoribbons with the lowest electronic bands given by $E_{\pm}(k) = \pm \hbar v_F |k|$. In these metallic nanoribbons, although the electron wave functions favor forward scattering, they are not localized around the two ribbon edges. As a result, the polarization retains time-reversal symmetry. For metallic graphene nanoribbons, we obtain the interband polarization function

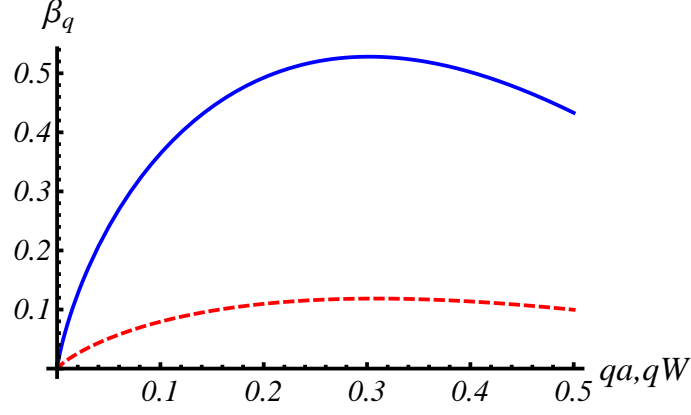


FIG. 6: (Color online) Plasmon weight β_q for TI-based (blue solid curve) and conventional (dashed red curve) 1DEGs, where ω_0 is chosen as the same for both cases.

$$\begin{aligned}
 \chi_1(q, \omega + i0^+) &= \Pi_{-1,+1}(q, \omega + i0^+) + \Pi_{+1,-1}(q, \omega + i0^+) \\
 &= \frac{1}{\pi} \left[\frac{q}{\hbar\omega - \hbar v_F q + i0^+} - \frac{q}{\hbar\omega + \hbar v_F q + i0^+} \right] \\
 &= \frac{2}{\pi} \frac{\hbar v_F q^2}{(\hbar\omega + i0^+)^2 - (\hbar v_F q)^2}.
 \end{aligned} \tag{17}$$

At the same time, the intraband polarization functions, $\Pi_{-1,-1}(q, \omega + i0^+)$ and $\Pi_{+1,+1}(q, \omega + i0^+)$, vanish due to time-reversal symmetry. This, in turn, results in the plasmon dispersion in Eq. (15) with electron Fermi velocity independent of the electron density. In other words, we have $v_F = \text{const}$ as in the case of 2DTI. Except for the spin factor of 2, the polarization function in Eq. (17) is identical to the two-component HL in 2DTI (i.e., both electron spin states are excited). From Eqs. (12), (15) and Fig. 4, one can easily understand that the energies of the collective excitations for the two and single component HLs are well separated in spectrum, but they share the same particle-hole excitation region.

For graphene, the plasmon excitations in doped semiconductor armchair nanoribbons are similar to the conventional 1DEG plasmon dispersion. The localization of electron wave functions along two ribbon edges can be obtained in zigzag nanoribbons. However, the cone-like band structure disappears for this case. Moreover, the particle-hole excitations cover a broad region, instead of a narrow line, and the plasmon dispersion which falls into this broad region becomes Landau damped.

IV. CONCLUDING REMARKS

The dispersion of intraband plasmon excitations in a semi-infinite inverted HgTe/CdTe quantum well has been derived within the random-phase approximation based on a calculated edge-localized topological state of electrons in a single-component helical liquid using the BHZ model. Under the perturbation from a linearly-polarized incident light, the unique properties in the collective excitation of these edge-bound electrons with a broken time-reversal symmetry has been explored. Our calculations predict the plasmon dispersion $\omega_p(q) \sim -\omega_0 q \ln(qa)$ for such a single-component helical state in the long-wavelength limit, in sharp contrast with $\omega_p(q) \sim -\omega_0 \sqrt{-\ln(qW)}$ found for a one-dimensional electron gas in a quantum-wire system. Moreover, ω_0 in our plasmon dispersion is independent of the linear electron density, similar to the case for a metallic armchair graphene nanoribbon. On the other hand, the plasmon dispersion of the two-component helical liquid is found to be identical to that of a armchair graphene nanoribbon except for the spin prefactor and a characteristic-width scaling of the wave number. The particle-hole excitation region shrinks into a straight line in our system, in comparison with a wide region for a conventional one-dimensional electron gas. The plasmon energy of the single-component helical state is well separated from that of the two-component helical state but they share the common particle-hole excitation region in the excitation spectrum.

Acknowledgments

This research was supported by the contract # FA 9453-07-C-0207 of AFRL. DH would like to thank the Air Force Office of Scientific Research (AFOSR) for its support.

-
- [1] X. Qi and S. Zhang, Reviews of Modern Physics **83**, 1057 (2011).
 - [2] J. McIver, D. Hsieh, H. Steinberg, P. Jarillo-Herrero, and N. Gedik, Nat. Nanotechnol. (in press) (2012).
 - [3] M. König, H. Buhmann, L. Molenkamp, T. Hughes, C. Liu, X. Qi, and S. Zhang, Journal of the Physical Society of Japan **77**, 031007 (2008).
 - [4] B. Bernevig, T. Hughes, and S. Zhang, Science **314**, 1757 (2006).
 - [5] S. Xu, Y. Xia, L. Wray, S. Jia, F. Meier, J. Dil, J. Osterwalder, B. Slomski, A. Bansil, H. Lin, et al., Science **332**, 560 (2011).
 - [6] S. Raghu, S. Chung, X. Qi, and S. Zhang, Physical review letters **104**, 116401 (2010).
 - [7] D. Efimkin, Y. Lozovik, and A. Sokolik, Arxiv preprint arXiv:1107.4695 (2011).
 - [8] S. Sarma, S. Adam, E. Hwang, and E. Rossi, Reviews of Modern Physics **83**, 407 (2011).
 - [9] D. H. Huang, Y. Zhu, and S. X. Zhou (???)
 - [10] L. Brey and H. Fertig, Physical Review B **75**, 125434 (2007).
 - [11] S. Sarma and E. Hwang, Physical Review B **54**, 1936 (1996).
 - [12] C. Wu, B. A. Bernevig, and S.-C. Zhang, Phys. Rev. Lett. **96**, 106401 (2006).
 - [13] K. Imura, A. Yamakage, S. Mao, A. Hotta, and Y. Kuramoto, Physical Review B **82**, 085118 (2010).
 - [14] Q. P. Li and S. Das Sarma, Phys. Rev. B **43**, 11768 (1991).
 - [15] Y. Zhu, D. H. Huang, and S. Feng, Phys. Rev. B **40**, 3169 (1989).
 - [16] Q. P. Li, S. Das Sarma, and R. Joynt, Phys. Rev. B **45**, 13713 (1992).